Enhancement of Topographic Images Obtained in Liquid Media by Atomic Force Microscopy

Younghun Kim[†] and Jongheop Yi*[,‡]

Department of Chemical Engineering, Kwangwoon University, 447-1, Wolgye, Nowon, Seoul 139-701, Korea, School of Chemical and Biological Engineering, Seoul National University, San 56-1, Shillim, Kwanak, Seoul 151-742, Korea

Received: June 9, 2006; In Final Form: August 28, 2006

The open liquid-cell atomic force microscope (AFM) has potential for studies of biomaterials and surface morphology in liquid media, and a variety of fluids can be used as buffer solutions. The dependence of image distortion on fluid properties (kinematic viscosity) has been studied with edge friction force obtained in lateral images and will shortly appear elsewhere [*Appl. Phys. Lett*. **2006**, *88*, 173121]. Previous studies indicate that the scan rate should be slower for obtaining a nondistorted image. However, the time required for the scan is greatly increased. Therefore, we introduced the vector concept to evaluate the net force for scanning in the *y*-direction and found two solutions to achieve a zero force difference introduced by the cantilever−fluid and the tip−surface. When the scan rate approaches zero or a specific velocity (30 μm/s in this study), the force of the interaction induced by the cantilever−fluid and tip−surface is reduced to a considerable extent. Among the two solutions, a scan with a specific velocity is an easy, rapid method for obtaining a nondistorted image, compared to the previously proposed method (scan rate approaches zero). This proposed model was confirmed in a proof-of-concept test using 2-propanol.

Introduction

Liquid atomic force microscopy (AFM) is a convenient tool for the study of biological samples in their native environment,[1,2] in situ observations of structural changes,[3,4] and nanopatterning in an organic phase.[5,6] In general, AFM permits high-resolution images to be obtained in air, but a meniscus force, induced by the condensation of water between tip and sample, can have an effect on the imaging force, namely a van der Waals force.[7] Because both the cantilever and tip is immersed in water in liquid AFM, the meniscus force induced by the condensation of water in air conditions can be eliminated, and thus nondistorted images can be obtained. Therefore, liquid AFM is well-known as a suitable method for imaging soft materials such as biomaterials and thin films.

This feature, however, was corrected only when water is used as a liquid medium. For studies of biomaterials or the observation of a self-assembled monolayer in real time, various liquids have been used as buffer solutions. PEG, polyelectrolytes, and octane as a liquid medium in liquid-cell AFM have been used for imaging biomaterials,[1] thin films,[4] and patterning,[8] respectively. When a standard grating sample (TGX01, MikroMasch, Estonia) is analyzed in an inert organic phase, which is not water, in the contact-mode, the resulting images show some distortion, as shown in Figure 1. This image distortion is due to forces that develop between the tip and the sample in a filled liquid channel. The net force between the cantilever and sample is strongly dependent on the kinematic viscosity of the fluids. Therefore, the choice of an appropriate fluid is important in open liquid-cell AFM, in which nondistorted and real images are needed. The dependence of image distortion on fluidic properties has been summarized elsewhere.[9]

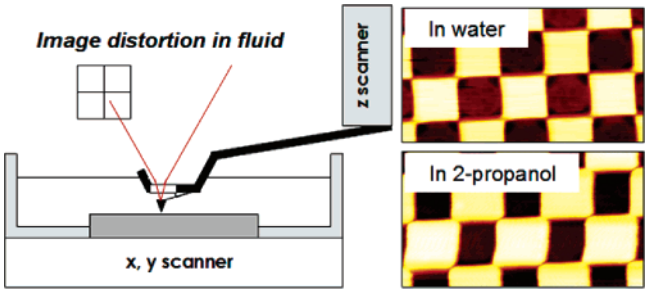

Figure 1. Configuration of open liquid-cell AFM and the topography of a grating sample obtained in water and 2-propanol.

Herein, we describe a modified squeeze−drag superposition model for a detailed elucidation of image distortion and conduct an enhancement test for the topographic image of a grating sample obtained in 2-propanol media as a proof-of-model. The open liquid-cell system[10] used in this work guaranteed the easy exchange and no-overflow of the solution as compared to closed[11] or solution-dropped[2] liquid-cell AFM. The reliability of image obtained through open liquid-cell system was investigated, and the noise levels (RMS, root-mean-square) for mica in air and water were monitored.

Theory

Local fluid−substrate force interactions with resolutions in the range of picoNewtons have been reported elsewhere.[12,13] Most of the data reported have been discussed mostly in terms of the interaction (F_{net1}) between the cantilever and substrate/fluid, quantified with the tip approaching the sample in the *z*-direction (V_z). It has been compared with theoretical models for squeeze−film effects (F_{sc}) and the drag (F_d) on AFM

* Corresponding author. E-mail: jyi@snu.ac.kr. Telephone: +82-2-880-7438. Fax: +82-2-885-6670.
† Department of Chemical Engineering, Kwangwoon University.
‡ School of Chemical and Biological Engineering, Seoul National University.

10.1021/jp063591+ CCC: $33.50
Published on Web 10/04/2006

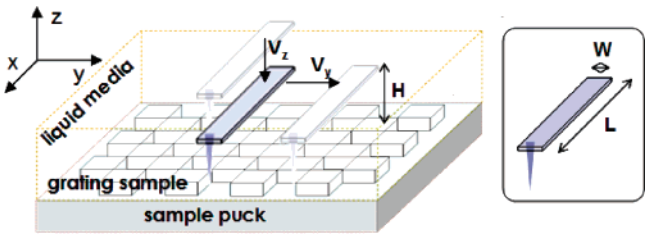

Figure 2. Schematics of a cantilever moving during tip approach with V_z (case 1) and scan with V_y (case 2).

cantilevers.[12] In this study, the net force acting in tip scanning (F_{net2}) in the y-direction (V_y) was obtained by the modification of F_{net1} with the shear force for coquette flow (F_c) and surface friction of the tip (F_f), represented by a modified squeeze−drag superposition model using the Navier−Stokes equation. A schematic of the required system variables is shown in Figure 2.

During tip approach with V_z. Herein, the reported equations[12] for the net force acting in the tip-approaching in the z-direction were modified. As a first step, water resistance was quantified in order to determine the increase in net forces. A submersed moving object (cantilever) in a fluid is affected by the drag force (F_d), which was approximated on the rectangular cantilever with the width (W) of the beam as the diameter for determining the drag coefficient (C_d). The resulting force acting on the cantilever is given by the expression:

$$F_d = C_d PA = C_d \frac{1}{2}\rho V_z^2 LW = \frac{8\pi}{\mathrm{Re}\log\left(\frac{7.4}{\mathrm{Re}}\right)}\frac{1}{2}\rho V_z^2 LW = \frac{4\pi\mu LV_z}{\log\left(\frac{7.4}{\mathrm{Re}}\right)} \quad (1)$$

where Re represents the Reynolds number, $\mathrm{Re} = \rho W V_z/\mu$. The pressure ($P$) was obtained from the z-component of the Navier−Stokes equation.[14,15] The drag coefficient for an AFM cantilever as a cylindrical body have been developed by many investigators[12] and was also used here.

When the cantilever approaches the surface, the liquid film of incompressible fluid between the cantilever and substrate is squeezed out. The squeeze−film force was calculated from the Stokes equation, assuming an incompressible and Newtonian fluid. With appropriate boundary conditions, the y-component of the Stokes equation becomes

$$0 = -\frac{\partial P}{\partial y} + \mu\frac{\partial^2 V_y}{\partial z^2} \quad \text{with } \frac{\partial V_y}{\partial z} = 0 \text{ at } z = 0 \text{ and } V_y = 0 \text{ at } z = H \quad (2)$$

Equation 2 gives

$$V_y = \frac{1}{2\mu}\frac{\partial P}{\partial y}(H^2 - z^2) \quad (3)$$

The pressure gradient and V_z are evaluated by using the continuity equation

$$\frac{\partial V_y}{\partial y} + \frac{\partial V_z}{\partial z} = 0 \text{ or } V_z = -\int_0^z \frac{\partial V_y}{\partial y} dz \quad (4)$$

To evaluate the integral we need to know how V_y and therefore $\partial P/\partial y$ is dependent on y.

$$\frac{\partial P}{\partial y} = yf(t) \text{ and } V_y = \frac{1}{2\mu} yf(t)(H^2 - z^2) \quad (5)$$

It is found that

$$V_z = \frac{1}{2\mu} f(t)\left(zH^2 - \frac{z^3}{3}\right) \text{ and thus } f(H) = \frac{3\mu V_z}{H^3} \quad (6)$$

The pressure gradient is now obtained by evaluating eqs 5 and 6 at $y = W$, where $P = 0$.

$$P = \frac{3\mu V_z}{2H^3}(W^2 - y^2) \quad (7)$$

The applied force for the entire cantilever is given by

$$F_s = \int P\, dA_z = \int_0^W \int_0^L P\, dx\, dy = \frac{\mu LV_z W^3}{H^3} = \frac{\mu LV_z}{S^3} \quad (8)$$

The final equation should be corrected for the deflection of the cantilever to reflect the flexibility of an end-loaded cantilever with spring constant.[12] The corrected squeeze−film force with a normalized gap ($S = H/W \ll 1$) is expressed as follows:

$$F_{sc} = \varpi k_c = \frac{3F_s}{8k_c} k_c = \frac{3}{8}\frac{\mu LV_z}{S^3} \quad (9)$$

Therefore, F_{net1} consists of a drag force (F_d) and a squeeze−film force (F_{sc}), which is considered to be the cantilever deflection during the approach of the tip to the sample.

$$F_{net1} = F_d + F_{sc} = \mu LV_z\left(\frac{4\pi}{\mathrm{Log}\left(\frac{7.4}{\mathrm{Re}}\right)} + \frac{3}{8S^3}\right) = f(\mu, \rho, V_z, H) = f(\nu, V_z, H) \quad (10)$$

During scan with V_y. During a scan with V_y, two different forces are activated; the first corresponds to the force of the cantilever activated in the fluid due to the moving of the cantilever with V_y, and the second corresponds to the force of the tip activated by friction between tip and substrate due to the contact-mode. The two activated forces are referred to as $F_{\text{cantilever−fluid}}$, and $F_{\text{tip−surface}}$, respectively. The former can be derived by procedure similar to that used for F_{net1} and consists of a drag force (F_d), a squeeze−film force (F_{sc}), and a shear force (F_c). The latter, the friction force of the tip, was not represent in F_{net1} and can be defined as the sum of the shear stress (F_f) by tip contact and the loaded force (F_n). Therefore, $F_{\text{cantilever−fluid}}$ and $F_{\text{tip−surface}}$ represent the activated force by the cantilever and the tip, respectively.

The net force acting in the tip-scanning in the y-direction was modified from the F_{net1}. The drag force on a cantilever in y-directional scanning is similar to that for z-directional approaching, except that the contact is a different area. The thickness of the cantilever is typically 1 μm, 35 times smaller than its width. The resulting drag force is given by

$$F_d = C_d PA_y = C_d \frac{1}{2}\rho V_y^2 L\frac{W}{35} = \frac{4\pi\mu LV_y}{35\log\left(\frac{7.4}{\mathrm{Re}}\right)} \quad (11)$$

The squeeze−film force was obtained from the y-component of the Stokes equation.

$$0 = -\frac{\partial P}{\partial y} + \mu\frac{\partial^2 V_y}{\partial y^2} \text{ and thus } P = \frac{2\mu L V_y}{W} \quad (12)$$

After correction for the deflection of the cantilever,

$$F_{sc} = \frac{3F_s}{8} = \frac{3}{8}\left(\frac{2\mu L V_y}{W}\right)A_z = \frac{3\mu L V_y}{4} \quad (13)$$

For the plane surface in a laminar flow of a viscous liquid, tip-moving causes a surface-driven flow and activates a shear force.[15] In this force, the area of contact is A_z.

$$F_c = \frac{\mu V_y}{H} A_z = \frac{\mu L V_y}{S} \quad (14)$$

Therefore, the resulting forces ($F_{\text{cantilever}-\text{fluid}}$) between the cantilever and fluid for scanning are the sum of F_d, F_{sc}, and F_c.

The probe tip makes contact with the surface in contact-mode AFM. Consequently, an additional force as well as $F_{\text{cantilever}-\text{fluid}}$ was revealed with external loading force (F_n) and shear stress (τ), and that force ($F_{\text{tip}-\text{surface}}$) is induced between the tip and surface. The following equation describes the linear friction-load relationship.[13] The typical tip height (H_{tip}) of a NSC36B (k_c = 1.75 N/m, f_o = 155 kHz, MikroMasch, Estonia) is 15 μm, and thus the gap ($H-H_{tip}$)between the tip and surface was revised with the tip height.

$$F_f = \tau A_t + \alpha F_n = \frac{\mu V_y}{H-15} A_t + \alpha F_n \quad (15)$$

Where, A_t is the contact area for the tip, and can be obtained from the fact that the typical tip curvature radius of probe is ca.. 10 nm. The transition parameter (α) is a dimensionless coefficient in the range of 0−1.[16] Therefore, the final net force (F_{net2}) during the scanning of the sample consists of forces between the cantilever−fluid and the tip−surface, as follows.

$$F_{net2} = F_{\text{cantilever}-\text{fluid}} + F_{\text{tip}-\text{surface}} = (F_d + F_{sc} + F_c) + F_f$$

$$= \mu L V_y\left[\frac{4\pi}{35\log\left(\frac{7.4}{\text{Re}}\right)} + \frac{3}{4} + \frac{1}{S}\right] + \left(\frac{\mu V_y A_t}{H-15} + \alpha F_n\right) =$$

$$f(\mu, \rho, V_y, H) = f(\nu, V_y, H) \quad (16)$$

In the F_{net} equations, the main parameters for fluid properties are viscosity (μ) and density (ρ). To create a one-parameter system, kinematic viscosity ($\nu = \mu/\rho$) was introduced. To develop equations for net forces, several parameters, defined in Table 1, were used.

TABLE 1: Values for the Parameters Used in Eqs 10 and 16

parameters	value or range	unit	remark
cantilever length, L	90	μm	NSC36B tip
cantilever width, W	35	μm	NSC36B tip
velocity, V_z or V_y	0.1 to 10	μm/s	approaching or scanning
loading force, F_n	31.28	nN	contact mode
tip contact area, A_t	$\pi 10^2$	nm^2	NSC36B tip
gap between cantilever and surface, $H-15$	0.0005 to 10	μm	contact to noncontact
viscosity, μ; density, ρ	1.84×10^{-5}; 0.0012	Ns/m^2; g/cm^3	air
	0.001; 1.000		water
	1.201; 0.790		ethanol
	0.320; 0.789		acetone
	2.040; 0.790		2-propanol
	0.055; 0.790		methanol
	0.980; 0.779		cyclohexane

Experimental Methods

As illustrated in Figure 1, the open liquid-cell system is used in conjunction with a commercial AFM instrument (XE-100, PSIA, Korea). To minimize intrinsic distortion of the apparatus, an independent z-scanner was used, which also eliminates the $x-z$ cross-coupling problem that is inherent in conventional AFM.[17−20] The assembled system was tested for image distortion using a standard grating sample (TGX01, MikroMasch, Estonia) in various fluids, such as air, water, methanol, acetone, ethanol, cyclohexane, and 2-propanol in the contact mode. To enhance the image obtained in 2-propanol, the parameters for scanning were adjusted.

Results and Discussion

Checking the Noise Level in Open Liquid-Cell AFM. Generally, the mica provided a <1 nm roughness and thus is a suitable substrate for measuring the RMS of the system noise. We checked the noise level for mica in air and in water in the contact mode. As shown in Figure 3, mica has a very smooth surface. The roughness values in air and water were found to be 0.13 and 0.45 nm, respectively. The RMS was larger in the case of water than in air due to the interaction between the cantilever and substrate in the liquid media. The friction force between cantilever and substrate was increased with the kinematic viscosity of the liquid media. This suggests that the open liquid-cell system interfaced with a commercial AFM showed very small noise level during scans in water compared to air.

Net Force for the Tip-Approaching with V_z in the z-Direction. The net force (F_{net2}) for a tip-approaching with V_z regressed with the kinematic viscosity of various fluids when calculated using eq 10. As shown in Figure 4, as the approaching speed (V_z) increased, a higher net force was found between the cantilever and fluid. For a fluid with a high kinematic viscosity, this phenomenon becomes more clear.

In the contact AFM mode, an AFM tip makes soft "physical contact" with the sample. As is well-known in the interatomic force/distance curve, the distance between the tip and sample or repulsive region for the contact mode is typically 1−5 Å. When $H-15$ is 5 Å, the probe tip makes direct contact with a surface as a contact mode, while 10 μm is required for the full relaxation of the cantilever from the surface, and 2 μm of $H-5$ corresponds to the noncontact region. In the contact region, F_{sc} is larger than F_d, and the magnitude of F_{sc} approaches that of F_d far from the surface and then is reversed in the fully relaxed state. The height ($H-15$), of which F_{sc} comes to be the same as F_d for 0.1, 1, and 10 μm/s V_z are 6.27, 5.28, and 4.18 μm, respectively. Namely, as the approaching speed increases, F_{sc} becomes larger than F_d when the cantilever approaches the surface. It should be noted that the drag force (F_d) has an influence on the squeeze−film force (F_{sc}) at a wider range of height.

Although the kinematic viscosity is large, in the case of 2-propanol, its net force is similar to that of air or water when V_z is near 0.1 μm/s. The reason for this is due to the decrease in friction between the cantilever and fluid, as in the case of air or water. Therefore, if the force−distance ($F-D$) curve without external friction forces is needed, the approach speed for fluids with a high kinematic viscosity should be reduced to 0.1 μm/s.

The cantilever for the tip-approaching with V_z was moved from the noncontact regime to the contact regime in the z-direction. The noncontact mode introduced in this work is not the dynamic mode such as the tapping mode AFM and is usually

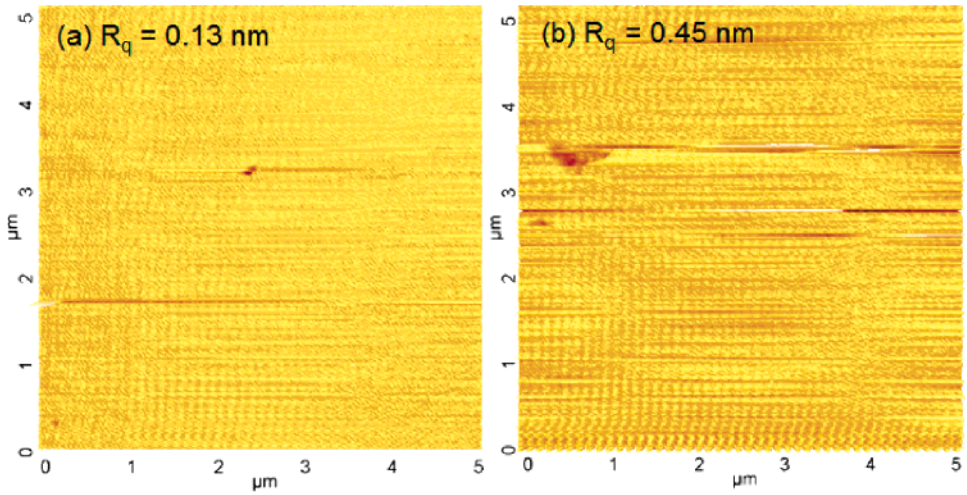

Figure 3. AFM images of mica (a) in air and (b) in water.

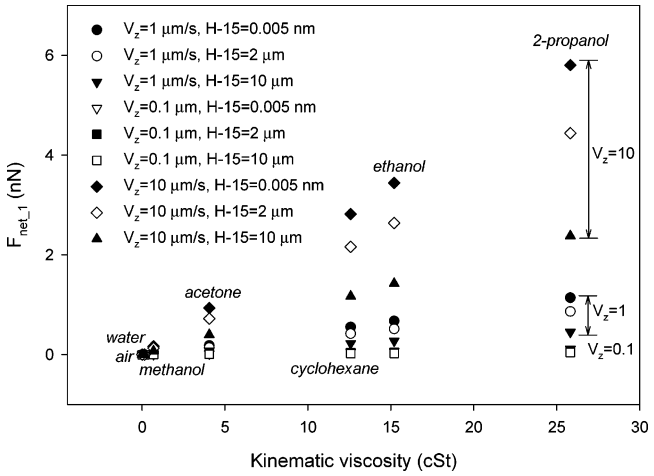

Figure 4. Dependence on the net force for tip-approaching kinematic viscosity with variations in the approaching rate (V_z) and the gap between the cantilever and surface ($H - 15$).

used to analyze the surface morphology at a contact *z*-height without vibration of the cantilever. When the tapping mode is used to analyze some samples in liquid media, the calculation of activated forces, F_{net2} as well as F_{net1}, are not easily derived from simple Navier−Stokes equations due to the dynamic motion of the cantilever. Therefore, in this work, proof-of-concept tests were conducted in contact-mode AFM, and the test and calculation for the tip-approaching with V_z was also performed, basically in the contact mode for measuring the $F-D$ curve. In this approaching/reproaching process for analyzing the $F-D$ curve, the gap between the tip and the surface was changed from the noncontact regime to the contact regime.

Figure 5 shows examples of $F-D$ curves measured (top) or calculated (bottom) in air, water, and ethanol media at 1 μm/s V_z. The negative value in the $F-D$ curve is due to the jump-to-contact phenomena of the tip to the surface, indicating that an attractive force such as van der Waals is acting between the tip and surface. The $F-D$ curve for air was larger compared to that for water and ethanol. Even in the case of ethanol, the attraction force was less due to diminishment by repulsive forces (drag−and squeeze−film). Namely, large F_{net1} of a cantilever in a fluid reduced the van der Waals attractions near the surface (contact region). Therefore, the hysteresis region (jump-to-contact) in the $F-D$ curve for ethanol, with a high kinematic viscosity, is small compared to that for air and water with small values. In Figure 5 (bottom), the height required to achieve the same F_{net1} is increased with increasing kinematic viscosity. This feature is consistent with experimental data at the top in Figure 5.

Net Force for Scanning with V_y in the *y*-Direction. In previous work, the correlation of edge friction force obtained for a lateral image and the kinematic viscosity of fluids was briefly reported elsewhere.[9] We found that the scan rate (V_y) should be decreased when a scan is performed in a fluid with a high kinematic viscosity. This was confirmed by measuring the noise level of a single-line scan with different V_y. The noise level of a single-line scan was induced by the friction of a fluid−cantilever and/or the tip−surface and acts as criteria for judging the possibility of obtaining a nondistorted image. Because a high noise level means a high possibility of obtaining a distorted image, several parameters for the scan should be adjusted before the start of the scanning. The data in Figure 6 were obtained in ethanol media and show that the noise level decreases with a decrease in scan rate.

Net Force for Scanning Corrected by Vector Force. To obtain real images with less noise, the choice of an appropriate fluid is important and a slow scan is required when fluids with a high kinematic viscosity are used. For a fluid with a higher kinematic viscosity, the time required to scan, however, is greatly increased, a time-consuming issue. To overcome this drawback, the concept of direction was added in eq 16.

The force induced in a moving fluid intrinsically has the concept of direction, namely a vector. During a scan with V_y in the *y*-direction, the vector direction of the friction force (F_{ts}) between the probe tip and surface acts with one of V_y. Therefore, eq 16 could be defined with a vector as follows.

$$\vec{F}_{net2} = \vec{F}_{cf} + \vec{F}_{ts} = \vec{F}_{cf} - \vec{F}_{ts} \qquad (17)$$

As described in eq 17, a velocity in which the sum of two vectors becomes zero is possible. Therefore, nondistorted and real images could be obtained if the specific velocity (V_{ys}) can be found.

The transition parameter (α) is a coefficient for defining the effective force of the loaded force (F_n) in $F_{tip-surface}$ and thus needs to be defined in order to find a specific solution (V_{ys}). α is in the range of 0−1 and describes the range of surface forces. For interaction forces per unit area, several models such as Hertz, JKR (Johnson−Kendall−Roberts), and DMT (Derjaguin−Müller−Toporov) have been developed.[13,16] There is no attractive force in the Hertz model. The JKR model takes short-range adhesion into account compared to elastic deforma-

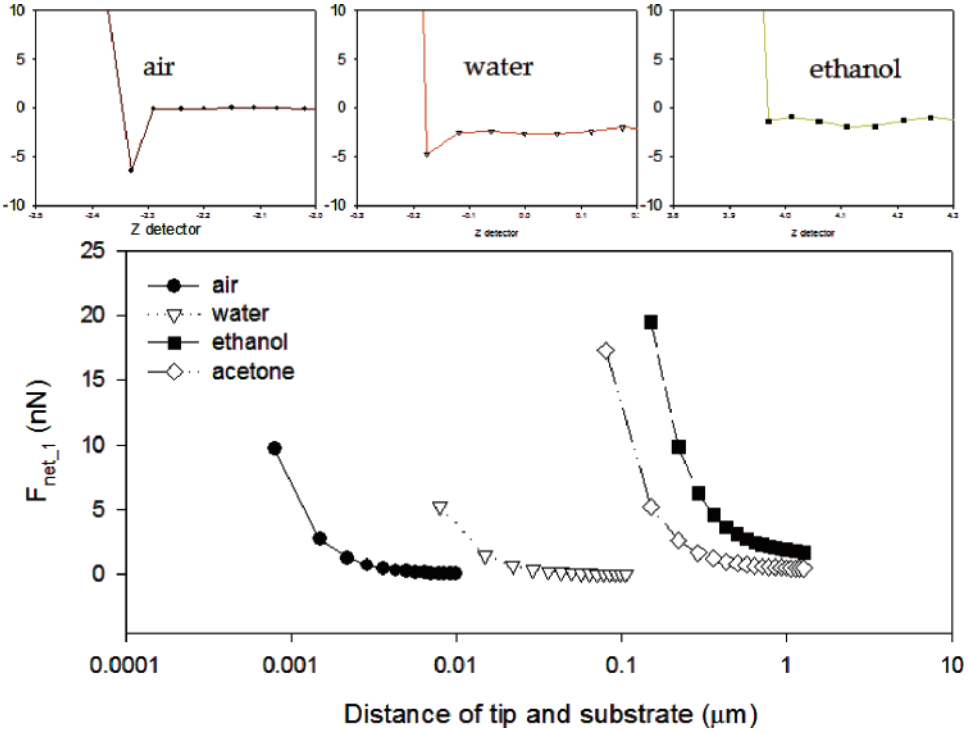

Figure 5. Measured (top) and calculated (bottom) force−distance curves in air, water, and ethanol.

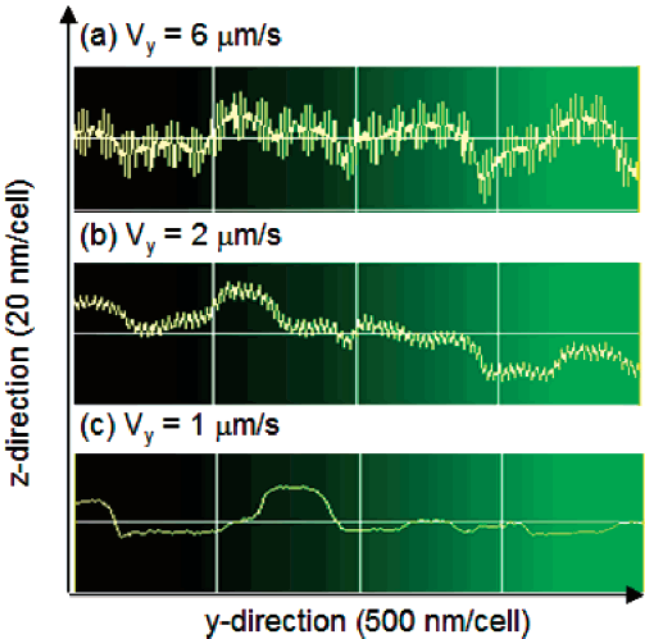

Figure 6. Noise level measured in ethanol at different scan rates.

tions. The DMT model represents a long-range surface force for stiff materials with a weak adhesion and small tip radii.[13] Except for the Hertz model, in both models, the friction force is proportional to the contact area (A_t) between the tip and the surface, and the transition parameter is dependent upon A_t.[16] When the scan rate is slow, the contact area of the tip on the surface is the same as the area of the tip curvature. In the case of a fast V_y, the contact area per unit time is increased. Therefore, the transition parameter is also dependent on the scan rate. In addition, the contact area is correlated with the viscosity of a fluid. Consequently, the transition parameter has the following correlation.

$$\alpha = f(A_t) = f(V_y,\nu) \tag{18}$$

where the range of α is 0−1, and α = 0 and 1 correspond exactly to the DMT and JKR cases, respectively.

Because α cannot be over 1, irrespective of whether V_y is greatly large or not, the function of α with V_y follows a sigmoidal or hyperbola curve with a single rectangular equation. The transition parameter has a following correlation with V_y and ν. Herein, a hyperbolic curve with a single rectangular equation was used.

$$\alpha = \frac{2V_y}{1 + (100/\nu)V_y} \tag{19}$$

Both the numerator and denominator in eq 19 have the same dimension, namely velocity (μm/s), and thus α becomes a dimensionless coefficient. Herein, 2 is the experience constant, and 100 is a correlation coefficient for kinematic viscosity. The experience constant in the numerator is also nondimensional. The term "1" has a dimension of velocity (μm/s) to reveal the limitation of transition parameter. If V_y is larger than ν/100, the transition parameter reaches a limitation value (ν/50). In liquid AFM, a long-range surface force induced by the liquid media between the cantilever and surface influence the transition parameter, and this feature is similar to the DMT model, which usually represents stiff materials with a weak adhesion and small tip radii. The proof-of-concept test in this study used the stiff grating sample, and thus, the transition parameter is nearly one for the DMT model. When the experience constant is above 2, the value of α approaches 1 under conditions of fast V_y and high υ. Even if the value is above 4, α exceeds the maximum value, 1. The correlation coefficient for kinematic viscosity was introduced to match the dimension in $1/\upsilon$, a function of the transition parameter, and has the dimension of cm^2/s. The value of α approaches the maximum value of α (α_{max}) with increasing V_y, and this feature is correlated with the kinematic viscosity. A small ν favors a small α_{max}, and the velocity to reach α_{max} is slower compared the case of a large ν. Therefore, for a small ν, α is almost constant over a wide range of V_y, namely less

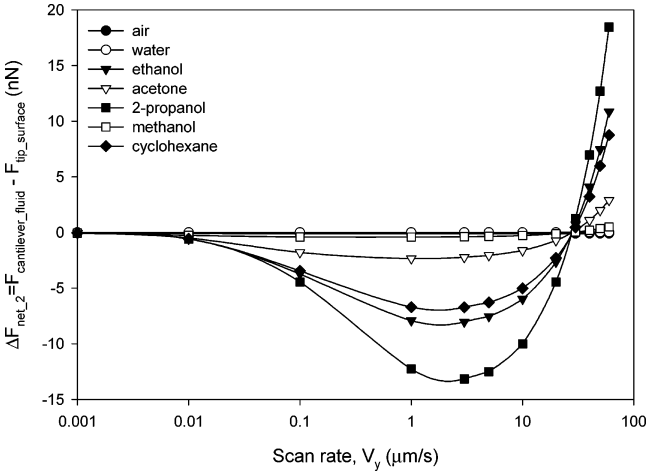

Figure 7. Difference in the net force for scanning with V_y in different fluids.

dependence upon V_y. Introducing eq 19 into eq 17, the difference of F_{cf} and F_{ts}, namely, ΔF_{net2}, is shown in Figure 7.

As shown in Figure 7, ΔF_{net2} escapes from the zero vicinity when the *y*-scan is conducted in a fluid with a high kinematic viscosity. In the case of air, water, and methanol, the force difference with scan rate is crowded near the zero point and thus is independent of the wide range of V_y. It should be noted that the *y*-scan in a fluid with a low kinematic viscosity such as water and methanol has almost the same interaction as that conducted in air and is influenced less by the fluid, such as the buffer. However, the force difference for a fluid with a high kinematic viscosity showed some different features as compared to air or water and was negative below the specific scan rate (V_{ys}). This indicates that F_{ts} is dominant over F_{cf}. The reverse case was also found for over V_{ys}. This feature comes clear with a increase in kinematic viscosity, such as for 2-propanol. In addition, the force difference approaches the zero point if the scan rate reaches zero.

Therefore, as shown in Figure 7, there are two solutions for achieving a force difference of zero. One exists when V_y approaches zero, another is the specific velocity (V_{ys}), about 30 μm/s when the *y*-scan was conducted in 10 × 10 μm^2 in an appropriate fluid. If the scan rate in a fluid with a high kinematic viscosity is in the vicinity of zero or V_{ys}, or if the force difference enters into the stable range of zero to ±2 nN, the force acting on that fluid becomes similar to that of air or water. The stable range shows a negligible force for forming a distorted image, and thus, even in a scan in 2-propanol, the resulting image might be the same as that in air or water due to similar interaction forces in 2-propanol as compared to air or water. In the case of a higher kinematic viscosity, the slope at V_{ys} (ca. 30 μm/s) is larger, and the zone for the stable force (0 to ±2 nN) is reduced. Therefore, image distortions such as tilting or blurring can be predicted to occur in situations sensitive to the scan rate.

Image Enhancement by the Adjusting Scan Rate. As a proof-of-concept test, the scanning of a grating standard sample in 2-propanol was conducted at various scan rates. The resulting images are shown in the inset in Figure 8. The images obtained in the vicinity of zero and 30 μm/s showed nondistorted and real images, similar to that of air or water. However, the result of a scan at 1−10 μm/s V_y showed a distorted image with tilting, while at scan speeds over 30 μm/s V_y, the image was blurred. The former was due to the dominant F_{ts} between the tip and surface, which induced serious noise. The latter was due to the dominant F_{cf} between the cantilever and fluid, which originated from the fast moving of the cantilever.

Conclusion

Liquid AFM is a most useful tool for studying biomaterials or a morphological change in a surface by an in situ observation. However, scans in some fluids used as a buffer in liquid AFM show distorted images. This feature is induced by certain fluid properties, and we found that image distortion was correlated with the kinematic viscosity of the fluid used. An image scanned in a fluid with a higher kinematic viscosity resulted in seriously distorted results. To investigate this phenomenon, the modified squeeze−drag superposition model was used, and the conditions for removal of the force difference ($F_{cf} - F_{ts}$) were found. One

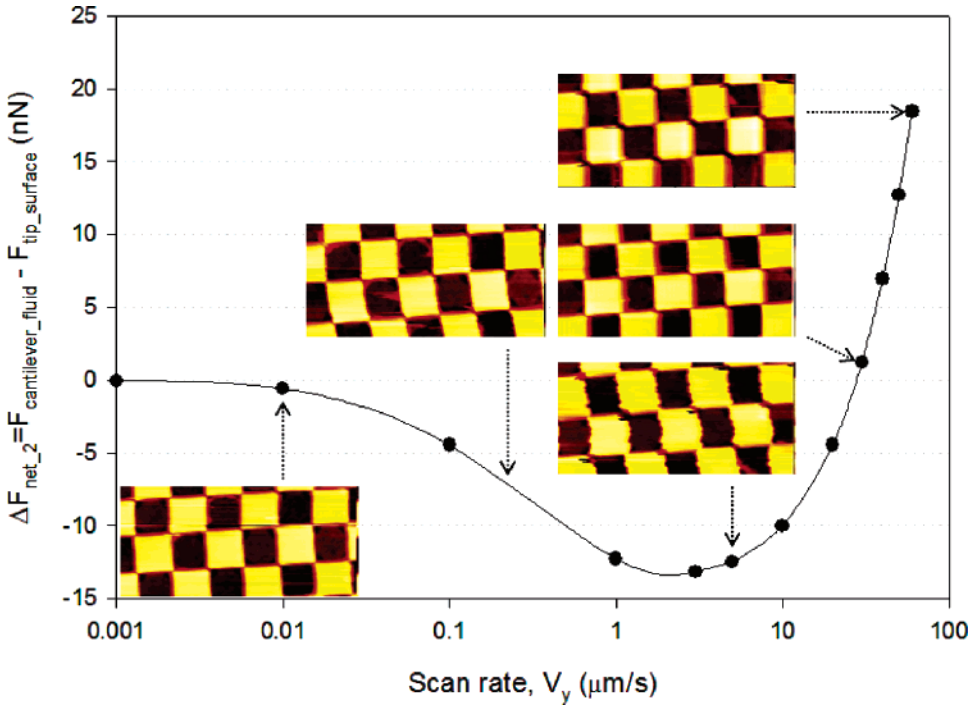

Figure 8. Calculated difference in the net force for scanning and a scanned image of standard grating sample in 2-propanol.

exists when V_y approach as zero, another is the specific velocity (V_{ys}), which was about 30 μm/s in this study. As shown in a proof-of-concept test, when the scan is performed in a fluid with a high kinematic viscosity, the scan rate should be decreased to zero or approach a specific velocity to reduce the effective force of the cantilever−fluid and the tip−surface.

Acknowledgment. We are grateful to the Basic Research Program (R01-2006-000-10239-0) of the Korea Science & Engineering Foundation for financial support. This research was conducted through the Research Grant of Kwangwoon University in 2006.

References and Notes

(1) Choi, I.; Kang, S. K.; Lee, J.; Kim, Y.; Yi, J. *Biomaterials* **2006**, *27*, 4655−4660.

(2) Kasas, S.; Wang, X.; Hirling, H.; Catsicas, S.; Haeberii, C.; Dietler, G.; Thomson, N. *Rev. Sci. Instrum.* **2000**, *71*, 4338−4340.

(3) Zhang, H.; Zhang, D.; He, Y. *Microsc. Res. Tech.* **2005**, *66*, 126−131.

(4) Menchaca, J.-L.; Jachimska, B.; Cuisinier, F.; Pérez, E. *Colloids Surf. A* **2003**, *222*, 185−194.

(5) Kim, Y.; Kang, S. K.; Choi, I.; Lee, J.; Yi, J. *J. Am. Chem. Soc.* **2005**, *127*, 9380−9381.

(6) Tello, M.; García, R. *Appl. Phys. Lett.* **2003**, *83*, 2339−2341.

(7) Arai, T.; Aoki, D.; Okabe, Y.; Fujihira, M. *Thin Solid Films* **1996**, *273*, 322−326.

(8) Kinser, C. R.; Schmitz, M. J.; Hersam, M. C., *Nano Lett.* **2005**, *5*, 91−95.

(9) Kim, Y.; Kang, S. K.; Choi, I.; Lee, J.; Yi, J. *Appl. Phys. Lett.* **2006**, *88*, 173121-1−173121-3.

(10) Kim, Y.; Choi, I.; Kang, S. K.; Lee, J.; Yi, J. *Rev. Sci. Instrum.* **2006**, *77*, 036114-1−036114-3.

(11) Mou, J.; Huang, G.; Shao, Z. *Rev. Sci. Instrum.* **1996**, *67*, 2654−2655.

(12) Jones, R. E.; Hart, D. P. *Tribol. Int.* **2005**, *38*, 335−361.

(13) Hurley, C. R.; Leggett, G. J. *Langmuir* **2006**, *22*, 4179−4183.

(14) *Transport Phenomena*; Bird, R. B., Stewart, W. E., Lightfoot, E. N., Eds.; Wiley: New York, 1960.

(15) *Analysis of Transport Phenomena*; Deen, W. M., Ed.; Oxford University Press: New York, 1998.

(16) Carpick, R. W.; Ogletree, D. F.; Salmeron, M. *J. Colloid Interface Sci.* **1999**, *211*, 395−400.

(17) Kwon, J.; Honh, J.; Kim, Y.-S.; Lee, D.-Y.; Lee, S.; Park, S. *Rev. Sci. Instrum.* **2003**, *74*, 4378−4383.

(18) Kim, Y.; Choi, I.; Kang, S. K.; Lee, J.; Yi, J. *Microelectron. Eng.* **2005**, *81*, 341−348.

(19) Kim, Y.; Choi, I.; Kang, S. K.; Lee, J.; Yi, J. *Appl. Phys. Lett.* **2005**, *86*, 073113-1−073113-3.

(20) Kim, Y.; Choi, I.; Kang, S. K.; Lee, J.; Yi, J. *Appl. Phys. Lett.* **2006**, *88*, 013113_1−013113_3.